ROTATION MEASURES ACROSS PARSEC-SCALE JETS OF FANAROFF–RILEY TYPE I RADIO GALAXIES

P. Kharb[1], D. C. Gabuzda[2], C. P. O'Dea[3], P. Shastri[4], AND S. A. Baum[5]
[1] Department of Physics, Purdue University, West Lafayette, IN 47907, USA; pkharb@physics.purdue.edu
[2] University College Cork, Cork, Republic of Ireland
[3] Department of Physics, Rochester Institute of Technology, Rochester, NY 14623, USA
[4] Indian Institute of Astrophysics, Koramangala, Bangalore 560034, India
[5] Center for Imaging Science, Rochester Institute of Technology, Rochester, NY 14623, USA

ABSTRACT

We present the results of a parsec-scale polarization study of three FRI radio galaxies—3C66B, 3C78, and 3C264—obtained with Very Long Baseline Interferometry at 5, 8, and 15 GHz. Parsec-scale polarization has been detected in a large number of beamed radio-loud active galactic nuclei, but in only a handful of the relatively unbeamed radio galaxies. We report here the detection of parsec-scale polarization at one or more frequencies in all three FRI galaxies studied. We detect Faraday rotation measures (RMs) of the order of a few hundred rad m^{-2} in the nuclear jet regions of 3C78 and 3C264. In 3C66B, polarization was detected at 8 GHz only. A transverse RM gradient is observed across the jet of 3C78. The inner-jet magnetic field, corrected for Faraday rotation, is found to be aligned along the jet in both 3C78 and 3C264, although the field becomes orthogonal further from the core in 3C78. The RM values in 3C78 and 3C264 are similar to those previously observed in nearby radio galaxies. The transverse RM gradient in 3C78, the increase in the degree of polarization at the jet edge, the large rotation in the polarization angles due to Faraday rotation, and the low depolarization between frequencies suggest that a layer surrounding the jet with a sufficient number of thermal electrons and threaded by a toroidal or helical magnetic field is a good candidate for the Faraday rotating medium. This suggestion is tentatively supported by *Hubble Space Telescope* optical polarimetry but needs to be examined in a greater number of sources.

Key words: galaxies: individual (3C66B, 3C78, 3C264) – polarization

Online-only material: color figures

1. INTRODUCTION

Knowledge of the ambient medium near the jet launching site in the central parsecs of an active galactic nucleus (AGN) can shed light on why these AGNs produce jets with different morphologies: low-luminosity Fanaroff–Riley type I radio galaxies (FRI; Fanaroff & Riley 1974) have jets that flare into diffuse radio lobes on scales of a few hundred parsec, while the narrow, collimated jets in the high-luminosity FR type II radio galaxies terminate in bright hot spots and create radio lobes via plasma backflow. Although the origin of the FR dichotomy is an open question, and a number of differences in the two classes have been cited as potential causes, differences in the nuclear environments of FRIs and FRIIs, which in turn influence the evolution of the jet due to interaction and entrainment, are widely believed to be important (e.g., Begelman 1982; Baum et al. 1995; Bicknell 1995; De Young 1996; Laing 1996).

Very long baseline interferometry (VLBI) is currently the only technique by which the parsec-scale environments of radio galaxies can be probed. Multifrequency polarization-sensitive VLBI experiments can determine the Faraday rotation measure (RM) arising in the vicinity of the parsec-scale radio jets. Radiation propagating through a magneto-ionic medium has its plane of polarization rotated from its intrinsic value χ_0 to χ following the relation

$$\chi = \chi_0 + \text{RM}\lambda^2 \qquad (1)$$

where

$$\text{RM} = 812 \int n_e B_\parallel dl \text{ rad m}^2 \qquad (2)$$

with n_e being the electron density in cm^{-3}, $B_\parallel$ the net line-of-sight magnetic field in milligauss, and dl an element of path length through the plasma in parsecs (see review by Gardner & Whiteoak 1966). The net parsec-scale RM is dominated by contributions from the nuclear environment of the AGN in its host galaxy and our own Galaxy; the Galactic contribution is usually estimated using arcsecond-resolution observations at multiple wavelengths near 18–20 cm (e.g., Rudnick & Jones 1983). VLBI RMs have been observed and studied in a number of relativistically beamed AGNs, i.e., radio-loud quasars and BL Lac objects. Such studies have indicated that contributions to the RM from regions close to the radio jets are dominant (e.g., Zavala & Taylor 2003, 2004).

Radio galaxies are believed to be the plane-of-sky counterparts of quasars and BL Lacs (Urry & Padovani 1995). Since their cores and jets are not as strongly Doppler boosted and are therefore radio faint, there have been relatively few VLBI polarization studies done on them, and polarization has been detected on parsec scales in only a handful (Taylor et al. 2001, 2006; Middelberg 2004; Zavala & Taylor 2002; Kharb et al. 2005). Parsec-scale RMs have only been estimated for the FRII radio galaxies 3C111, 3C120, and 3C166, and the FRI radio galaxies M87 and 3C84. Here we augment these data with the parsec-scale polarization images of three FRI radio galaxies—3C66B, 3C78, and 3C264, along with the RM images of the latter two.

We have adopted a cosmology in which $H_0 = 71$ km s^{-1} Mpc^{-1}, $\Omega_m = 0.27$, and $\Omega_\Lambda = 0.73$. The spectral indices α are defined such that the flux density S_ν at frequency ν is $S_\nu \propto \nu^{-\alpha}$.

2. THE FRI GALAXIES UNDER STUDY

We observed four FRI radio galaxies from a larger sample of radio-loud sources (Kharb & Shastri 2004) that possessed optical nuclei in their *Hubble Space Telescope (HST)* images (Chiaberge et al. 1999, 2000; Verdoes Kleijn et al. 2002), and had a correlated VLBI flux density ⩾100 mJy, with global VLBI at 8.4 GHz in 2002 March. Parsec-scale polarized emission was detected in all of them (Kharb et al. 2005). New observations of three of the four FRIs that showed polarization in their parsec-scale jets, viz., 3C66B, 3C78, and 3C264, were obtained at 5.0, 8.4, and 15.3 GHz in 2005 September with a global VLBI array including the VLBA and the Effelsberg antenna, and are the focus of the present work.

3C66B resides in an elliptical galaxy at a distance of 91 Mpc that forms a part of a dumbbell pair close to the Abell cluster 347. It is one of the few FRI radio galaxies in which the dominant radio jet has an infrared (Tansley et al. 2000), optical (Fraix-Burnet 1997), and an X-ray counterpart (Hardcastle et al. 2001). Kiloparsec-scale observations of 3C66B suggest the jet inclination to be less than ∼53° (Hardcastle et al. 1996), while an inclination for the VLBI jet of ∼45° has been inferred by Giovannini et al. (2001). X-ray observations have revealed the presence of copious amounts of hot gas, with which the kiloparsec radio jet seems to be interacting (Croston et al. 2003).

3C78 resides in the isolated, small E/S0 galaxy NGC1218 (Matthews et al. 1964) at a distance of 124 Mpc. *HST* observations have revealed that the optical galaxy has a face-on dust disk and an optical jet (Sparks et al. 1995). Baum et al. (1988) have reported that the innermost emission-line gas is elongated roughly in the direction of the radio jet, following the "alignment effect" (e.g., McCarthy et al. 1987; Privon et al. 2008).

The radio morphology of 3C264 is of the narrow-angle-tail type (O'Dea & Owen 1985). It is hosted by an S0 galaxy 93 Mpc away that lies in a dense part of the Abell cluster 1367 (Schombert 1986). Like 3C66B and 3C78, the radio jet in 3C264 also has an optical counterpart (Crane 1993). *HST* images show that the optical jet is projected onto a face-on dust disk (de Koff et al. 2000). A jet inclination angle of ∼50° has been inferred on kiloparsec (Baum et al. 1997, 1998) and parsec scales (Giovannini et al. 2001).

3. OBSERVATIONS AND DATA REDUCTION

Observations were carried out with the ten elements of the VLBA and the 100 m Effelsberg telescope at 5.0, 8.4, and 15.3 GHz on 2005 September 10, for a total of 24 h. The three radio galaxies were each observed for ≈2.5 h at each frequency. 3C84 was used as an instrumental polarization calibrator, assuming it to be unpolarized at these frequencies. The compact AGN 1156+295 was used as the electric vector position angle (EVPA or χ) calibrator. Five to six several-minute scans of each of these sources at each frequency were interspersed throughout the observing schedule.

The data were reduced using standard procedures in the Astronomical Image Processing System (AIPS) software package, using Los Alamos as the reference antenna at all stages of the calibration. Amplitude calibration was performed using the system temperatures and gain curve provided and the AIPS task APCAL, while the group delay and phase-rate calibration were performed using the AIPS task FRING. The cross-polarized delays were determined using the procedure VLBACPOL. Finally, the residual delays and delay rates were derived using FRING. The instrumental polarization leakage terms were determined

using the final self-calibrated map of 3C84 in the task LPCAL. These were typically of the order of 1%–2% at 5.0 and 8.4 GHz, and 1%–3% at 15.3 GHz for all the antennas.

We determined the absolute EVPA calibration by comparing the total VLBI-scale polarization of 1156+295 with integrated polarization obtained from monitoring databases maintained by the NRAO[6] and the University of Michigan Radio Astronomy Observatory (the latter data kindly provided by H. and M. Aller). Unfortunately, there were no integrated polarization measurements with good signal-to-noise ratio (S/N) available on the actual date of our VLBI experiment, making it necessary to interpolate these measurements to our VLBA date. This was straightforward for the 5 GHz EVPA calibration, since the NRAO database contained 5 GHz measurements on September 4 and 26 that virtually exactly coincided (differing by only 1° in the polarization angle χ, with errors in χ being 0.5°–1.5°). Accordingly, we adopted the integrated 5 GHz EVPA for 1156+295 to be −86° = +94°, and consider the overall uncertainty in our 5 GHz EVPA calibration to be no larger than 1°–2°.

NRAO measurements were also available at 8.4 GHz on these two dates, but showed a larger difference: $\chi = 81° \pm 1°$ on September 4, and 56° ± 3° on September 26. In addition, the UMRAO database had an 8 GHz measurement on September 24 with $\chi = 75° \pm 8°$; this latter measurement is of limited use due to its large uncertainty, although it suggests that the EVPA of 1156+295 was not wildly variable near the time of our VLBA observations. If the 25° change between the integrated EVPAs for the two NRAO measurements was fairly smooth, the 8.4 GHz EVPA on our observing date would have been 74°, and we adopted this as the integrated 8.4 GHz EVPA. This value is obviously somewhat uncertain; we accordingly consider the overall uncertainty in our 8.4 GHz EVPA calibration to be 3°–4°.

The NRAO polarization monitoring database does not include measurements at or near 15.3 GHz; the UMRAO database had two measurements near our VLBA observing date, but corresponding to very different χ values, each with relatively large uncertainties. Therefore, we explored two different ways to obtain an estimate of the integrated 15.3 GHz χ for our VLBA date: (1) obtain a linear fit of the polarization angle χ versus observing wavelength λ^2 for the 2005 September 4 NRAO data at 5, 8.4, and 22 GHz and use the resulting RM together with the reliably inferred 5 GHz integrated χ for 1156+295 on September 10 to derive a 15.3 GHz χ value for that date; (2) interpolate the NRAO 22 GHz χ values for 1156+295 for September 4 (63°) and September 26 (99°) in the same way that we did for the 8.4 GHz χ; (3) derive a χ versus λ^2 plot using the interpolated 5, 8.4, and 22 GHz polarization angles for September 10, and use the resulting RM for September 10 together with the reliably inferred 5 GHz χ value for 1156+295 for September 10 to derive a 15.3 GHz χ value for that date. In both cases, the plots of χ versus λ^2 could be approximated by linear fits within the errors. Approach (1) yielded $\chi_{15.3} \approx 68°$, while approach (2) yielded $\chi_{15.3} \approx 72°$. Realizing that some uncertainty in our EVPA calibration at 15 GHz was inevitable given in the limited calibration information, but encouraged by the fact that these two estimates were similar, we adopted an average value of 70°. We estimate the overall uncertainty in our 15.3 GHz EVPA calibration to be 5°–6°.

For reference, a total EVPA uncertainty of 6° between 5 and 8 GHz translates into an uncertainty in the corresponding RM

---

of about 45 rad m^{-2}. It is important to note that the application of an incorrect EVPA calibration will add the same offset to the observed EVPAs at every pixel in the map in which polarization is detected. Therefore, this can certainly bias the derived RMs, but cannot give rise to spurious RM gradients. Thus, although the absolute RMs that are derived will have some added uncertainty due to the uncertainty in our EVPA calibration, this is not propagated to an added uncertainty in the RM gradients.

The AIPS tasks IMAGR and CALIB were used iteratively for the imaging and self-calibration, respectively. Stokes Q and U maps were also made using IMAGR and the final, fully self-calibrated data. Pairs of the final Stokes I images at neighboring frequencies (5 + 8 GHz and 8 + 15 GHz) were made with identical beams, and used to derive spectral-index maps using the task COMB. Since information about the absolute position of the VLBI structure is inevitably lost during the phase self-calibration, it is necessary to first align the two I maps. The hybrid-mapping processes essentially align the VLBI cores, which is not the correct absolute alignment, since the core position is frequency dependent (Lobanov 1998). We determined the relative alignment between the pairs of I images based on a comparison of their optically thin regions of emission using the program of Croke & Gabuzda (2008); note that the algorithm used does not rely on the presence of distinct components at each frequency, and so is well suited to the images considered here.

The Stokes Q and U maps were used in the task COMB to obtain maps of the polarization intensity and polarization position angle. These polarization-angle maps at the different frequencies were used in either "COMB" or the task "RM" to obtain two-frequency or three-frequency RM maps, respectively. Prior to obtaining the RM maps, versions of the Q, U, and polarization-angle maps were made with identical beams. Polarization values with S/N less than three were blanked in COMB to produce the polarized intensity maps. The polarization-angle maps were restricted (by blanking in COMB) to have output errors less than $\approx 10°$. The three-frequency RM map of 3C78 was made using the AIPS task "RM," with unblanked polarization-angle maps and σ_{RM} blanking in "RM" such that $\sigma_{RM} < 55$ rad m^{-2}. Estimates for the peak surface brightness and the rms noise in the final total and polarized intensity maps were obtained using AIPS procedures TVMAXF, and TVWIN & IMSTAT, respectively. Depolarization maps were made using the degree of polarization maps at 5, 8, and 15 GHz for 3C78, and 5 and 8 GHz for 3C264. The polarization-intensity maps were first corrected for Ricean bias (e.g., Killeen et al. 1986) by using the AIPS task POLCO.

4. RESULTS

The total intensity radio images with polarization electric vectors superimposed are presented in Figures 1–3, the 5 and–8 GHz spectral-index maps in Figure 4 and RM maps and plots in Figures 5−8. Table 1 lists some parameters pertaining to the final images. We discuss our results for each radio galaxy below.

3C66B: our observations reveal tentative polarization close to the radio core only at 8 GHz, consistent with the epoch-2002 observations of Kharb et al. (2005). We failed to detect any polarization at 5 and 15 GHz. Simard-Normandin et al. (1981b) have listed an integrated RM of -67 ± 3 rad m^{-2}, corresponding to a rotation of about 5° at 8 GHz. The total intensity images at 5 and 8 GHz show a structure resembling a counterjet, as previously reported by Giovannini et al. (2001);

indeed, our spectral-index map shows the core region itself to be optically thick, but the emission to the southwest of the core to be optically thin. Using the jet-to-counterjet surface brightness ratio, $R_j = (\frac{1+\beta\cos\theta}{1-\beta\cos\theta})^p$ (Appendix A; Urry & Padovani 1995) at a distance of ~ 2 mas from the core, we obtain $\beta \cos \theta = 0.47$ for $R_j \sim 22$ and $p(= 2 + \alpha) = 3$. We can also estimate the Doppler factor, δ, using the ratio of the observed radio-core prominence parameter, R_c, to the intrinsic radio-core prominence, R_c^{int}, ($\delta = (\frac{R_c}{R_c^{int}})^{1/p}$; Urry & Padovani 1995), keeping in mind the caveat that R_c is a statistical measure of the orientation. Assuming R_c^{int} to be 0.33 and $R_c = 0.05$ for 3C66B (see Kharb & Shastri 2004), the above-derived $\beta \cos \theta$ gives a jet inclination angle of $\sim 60°$ for 3C66B.

3C78: among the three FRI radio galaxies considered here, 3C78 shows the most extensive polarization along its radio jet. We detect polarization in the jet at ~ 3 and 6 mas from the VLBI core at 5, 8, and 15 GHz. The 8 GHz image looks very similar to those from our epoch-2002 observations (Kharb et al. 2005) with the exception of a polarized core. We did not detect core polarization at any frequency in our present data. This is likely to be due to variability in the core, since our present image sensitivity is an improvement by a factor of ~ 1.5, over the 2002 observations. The total intensity images at 5 and 8 GHz show evidence for a counterjet, and this appears to be borne out by our spectral-index map, which shows the core to be optically thick, but the emission to the southwest of the core to be optically thin. The jet-to-counterjet ratio, R_j, varies from ~ 32 at ~ 1 mas to ~ 22 at ~ 2.5 mas. This results in $\beta \cos \theta$ varying from 0.52 to 0.47. Again assuming $R_c^{int} = 0.33$ and $R_c = 0.38$ for 3C78 (see Kharb & Shastri 2004), the derived $\beta \cos \theta$ results in a jet inclination angle of $\sim 50°$ for 3C78.

3C78 is the only one of the three radio galaxies for which the RM could be estimated using all the three frequencies. The RM in 3C78 ranges from about +200 rad m^{-2} to -400 rad m^{-2}. We observe an RM difference of > 300 rad m^{-2} transverse to the inner VLBI jet over a region that is ~ 5 mas (two beam sizes) across (Figure 5). As the EVPA rotates through almost 90° at the lower edge of the jet (Figure 5), the low-energy thermal electrons that produce the rotation cannot be completely mixed in with the synchrotron-emitting jet volume (Burn 1966; Cioffi & Jones 1980), and are therefore external to it. We discuss this further in Section 5. Figure 9 shows the polarization map of 3C78 after correcting for the RM. Since these regions are optically thin, the jet magnetic field is inferred to be aligned to the jet direction, in the region of the RM gradient. However, the magnetic field becomes orthogonal to the jet flow in the next jet component, and appears to remain orthogonal substantially further from the core (Figure 2, top left).

3C264: our observations reveal polarized emission at 5 and 8 GHz in two regions in the jet ~ 1 and 4 mas away from the core, similar to that observed by Kharb et al. (2005). We could obtain an RM map using only the 5 and 8 GHz maps. Therefore, the polarization angles are subject to $\pm n\pi$ ambituities, which are impossible to resolve. The two-frequency RM across the inner-jet varies from $\sim +250$ rad m^{-2} to ~ -300 rad m^{-2}. Note that an ambiguity of $\pm 180°$ between 5 and 8 GHz could result in an RM change of $\gtrsim \pm 2500$ rad m^{-2}. However, we find that the two-frequency RM in 3C264 is of the same order as the three-frequency RM in 3C78 and other radio galaxy jets (Table 2). Figure 9 shows the polarization map of 3C264 with the effects of the tentative two-frequency RM removed. If the two-frequency RM values are correct, the jet magnetic field is roughly aligned with the VLBI jet direction.
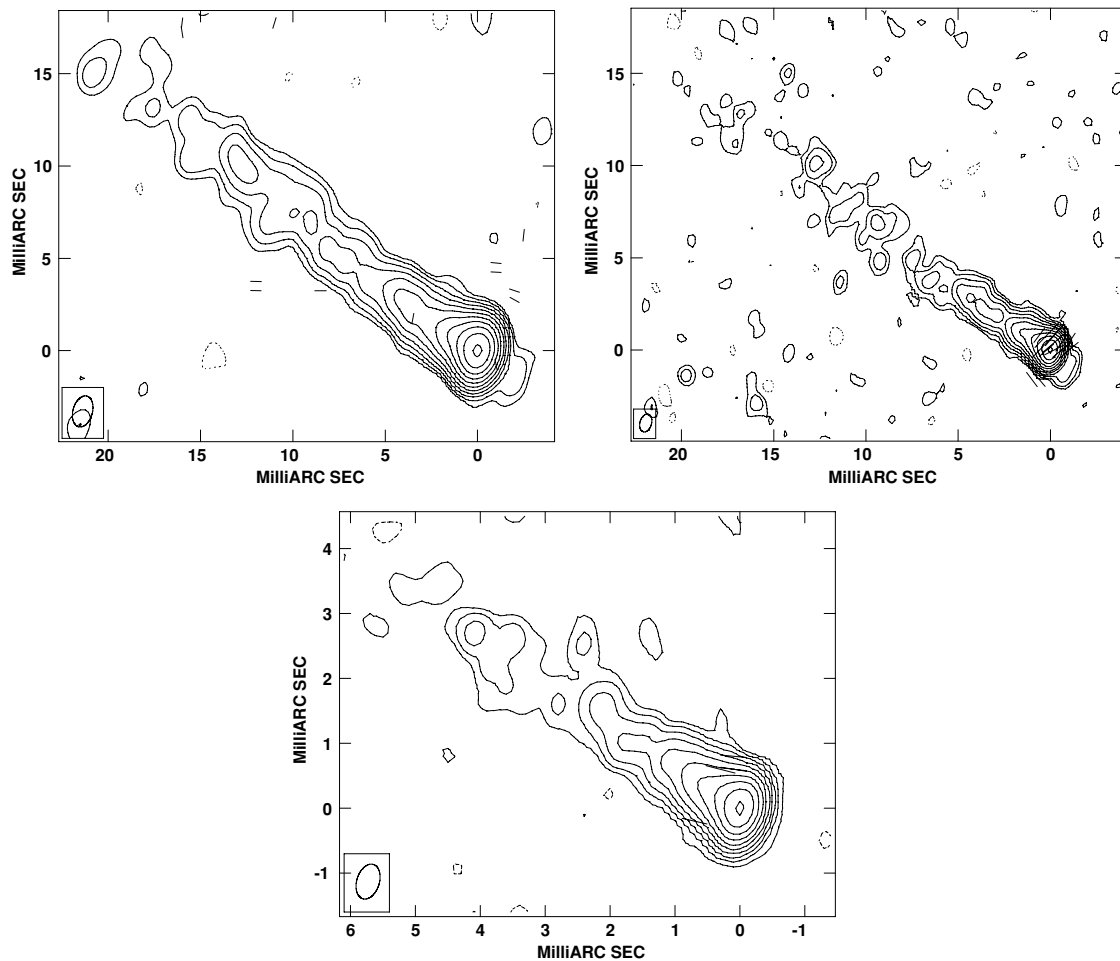
Figure 1. Total intensity maps of 3C66B at 5.0 GHz (top left), 8.4 GHz (top right), and 15.3 GHz (bottom) with polarization vectors superimposed. The contours are in percentage of the peak surface brightness and increase in steps of 2. The lowest contour and peak brightness for 5, 8, and 15 GHz are $\pm0.085\%$ of 114 mJy beam^{-1}, $\pm0.085\%$ of 111 mJy beam^{-1}, and $\pm0.085\%$ of 97 mJy beam^{-1}, respectively. χ vectors for 8 GHz: 1 mas = 0.3 mJy beam^{-1}.

4.1. Parsec-scale RM in Different AGN Classes

Prior to this study, parsec-scale RMs had been obtained for only the broad-line FRII radio galaxies 3C111 and 3C120 (Zavala & Taylor 2002), the narrow-line FRII radio galaxy 3C166 (Taylor et al. 2001), and the FRI radio galaxies M87 (Junor et al. 2001; Zavala & Taylor 2002) and 3C84 (Taylor et al. 2006). It is worth pointing out that 3C120 is a peculiar radio source. Although sometimes it has been classified as an FRI (e.g., Owen & Laing 1989), it possesses a quasar-like prominent broad-line spectrum (Tadhunter et al. 1993). Akin to FRII sources, it lacks counterjet emission and exhibits superluminal jet motion on scales of a few hundred parsecs (Walker et al. 1987). Table 2 lists all available VLBI RM estimates for the radio galaxies. A nonuniform parsec-scale RM distribution has also been observed in 3C166 (Taylor et al. 2001). A recent paper by Gomez et al. (2008) demonstrates a clear RM gradient across the jet in 3C120.

The absolute RM estimates for the parsec-scale jets of quasars and BL Lacs lie typically in the range of 100–500 rad m^{-2} (Zavala & Taylor 2004). This is interesting because the absolute parsec-scale jet RM values of the FRI and FRII radio galaxies studied so far, although few, fall in the same range. Further, the galaxies studied so far seem to reside in widely varying environments, from the center of clusters (e.g., 3C264) to being relatively isolated (e.g., 3C78). Therefore, the similarity in the

RM values across the parsec-scale jets of different classes of AGN suggests that the Faraday rotating medium is perhaps intrinsic and closely associated with the jet itself.

5. THE FARADAY ROTATING MEDIUM

5.1. Galaxy ISM

It has been clear from the earliest VLBI Faraday rotation measurements (e.g., Taylor 1998; Nan et al. 1999, 2000; Gabuzda et al. 2001; Reynolds et al. 2001) that the parsec-scale RM distributions are usually nonuniform, indicating that there must be a substantial component of Faraday rotation that is intrinsic to the AGNs, rather than arising in our own Galaxy or on larger scales in the host galaxy of the AGN (e.g., Taylor 1998; Udomprasert et al. 1997). The RM varies on scales of a few parsec in 3C78 and 3C264. The RM gradient across the VLBI jet of 3C78 is observed over a ~5 mas (~3 pc) region. Therefore, it is difficult to assign the role of the Faraday rotating medium to the ISM in our Galaxy or the radio host galaxy. Recent X-ray observations of elliptical galaxies (see Mathews & Brighenti 2003) suggest that the electron density of the hot gas in the centers is typically ~0.1 cm^{-3} and falls off with radius (r) as $n_e \propto r^{-1.25\pm0.25}$. Assuming that the RM is produced in the hot gas prevalent on scales of a 100 pc, it would produce an RM > 40000 rad m^{-2} for a uniform magnetic field, where the line-of-sight magnetic field strength is equal
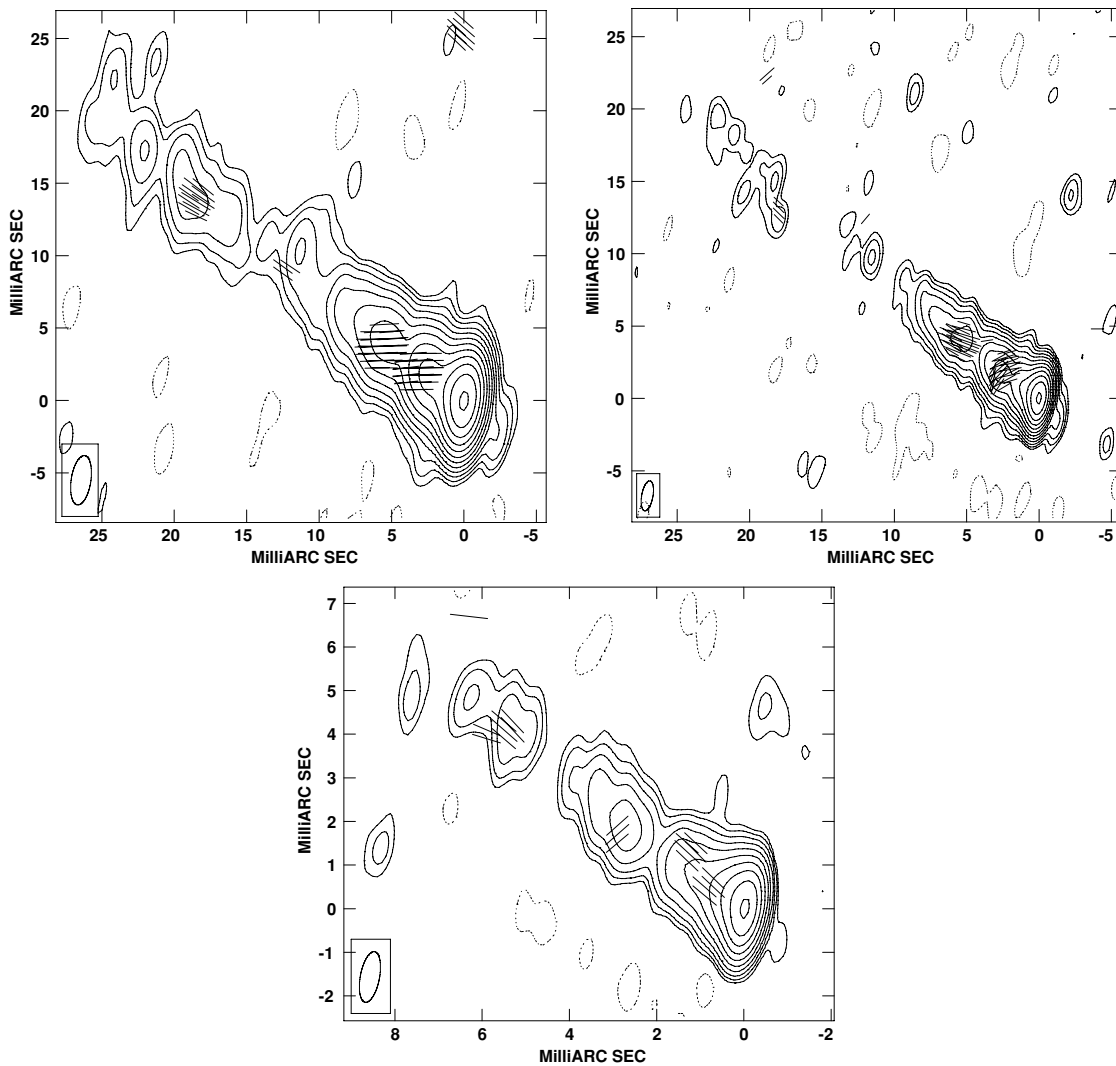
Figure 2. Total intensity maps of 3C78 at 5.0 GHz (top left), 8.4 GHz (top right), and 15.3 GHz (bottom) with polarization vectors superimposed. The contours are in percentage of the peak surface brightness and increase in steps of 2. The lowest contour and peak brightness for 5, 8, and 15 GHz are $\pm 0.042\%$ of 342 mJy beam^{-1}, $\pm 0.042\%$ of 331 mJy beam^{-1}, and $\pm 0.17\%$ of 242 mJy beam^{-1}, respectively. χ vectors for 5, 8, and 15 GHz: 1 mas = 0.25, 0.3, and 0.8 mJy beam^{-1}, respectively.

to the "equipartition" magnetic field (say ~ 5 mG, see Section 5.2). This is clearly not observed. However, if the magnetic field was not uniform and there were "N" reversals in the field direction along the line of sight, then the observed RM of ~ 200 rad m^{-2} would require $N > 40{,}000$. Such a large number of field reversals would however result in a net depolarization on parsec scales, which does not seem to be the case, as discussed below.

5.2. Radio Jet and Surrounding Medium

Considering the medium surrounding the parsec-scale jet: the broad-line region (BLR) has been inferred to have extents typically less than a parsec (Urry & Padovani 1995). BLR clouds could therefore be ruled out as a potential Faraday rotating medium for the jet region lying a couple of parsecs away from the core. The narrow-line region (NLR) could, however, extend to hundreds of parsecs and have a large covering factor ($\sim 30\%$–50%, Netzer & Laor 1993; Rowan-Robinson 1995). The NLR clouds could therefore in principle contribute to the observed RMs. However, the short timescale variability observed in the parsec-scale RM suggests that NLR clouds or the intercloud gas cannot be the primary Faraday rotating medium,

but rather this medium is closely linked with the relativistic jet itself (Asada et al. 2008a; Zavala & Taylor 2005).

We created depolarization maps for 3C78 and 3C264 using the relation $\mathrm{DP} = \frac{m_l}{m_h}$, where m_l, m_h are the degree of polarization maps at the lower and higher frequencies, respectively. We made DP maps for 3C78 between 5 and 8 GHz (polarized intensity maps were blanked below 10σ) and between 8 and 15 GHz (polarized intensity maps were blanked below 3σ). The mean 5–8 GHz and 8–15 GHz depolarization values in 3C78 in the region ~ 3 mas away from the core were $\mathrm{DP}_8^5 = 0.98 \pm 0.11$ and $\mathrm{DP}_{15}^8 = 0.79 \pm 0.15$, while in the region ~ 6 mas away they were $\mathrm{DP}_8^5 = 0.60 \pm 0.07$ and $\mathrm{DP}_{15}^8 = 0.64 \pm 0.09$. We note that the DP_{15}^8 value in the region closer to the core (~ 3 mas) was obtained over a much smaller region than DP_8^5. Overall these large DP values suggest that there was little depolarization at longer wavelengths in 3C78. The depolarization map for 3C264 was made using the degree of polarization maps at 5 and 8 GHz (polarized intensity maps were blanked below 5σ). The mean depolarization was $\mathrm{DP}_8^5 = 0.44 \pm 0.11$ around ~ 1 mas away from the core.

We noted in Section 4 that in 3C78, the polarization angle seems to rotate by almost $90°$ at the lower edge of the jet
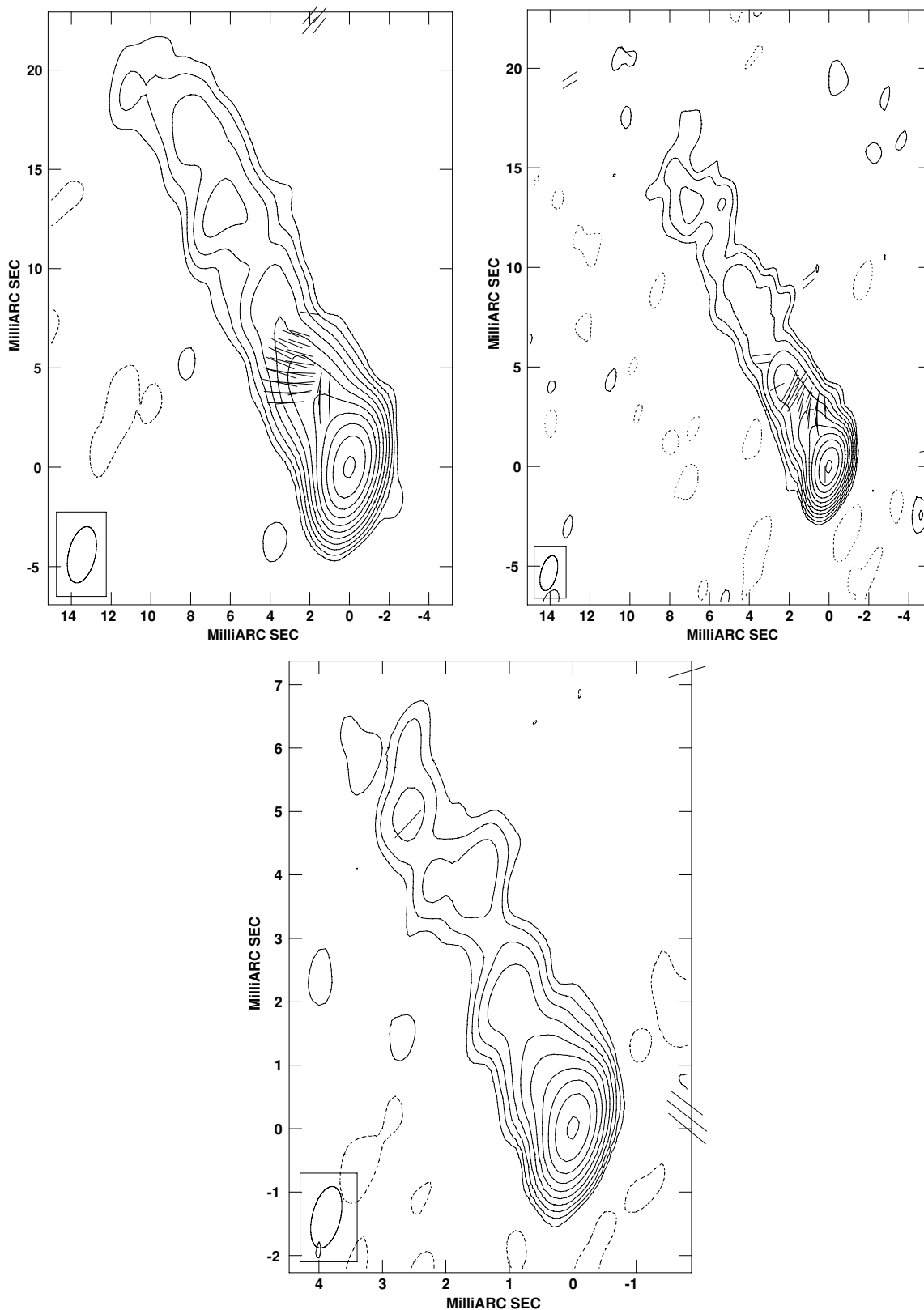
Figure 3. Total intensity maps of 3C264 at 5.0 GHz (top left), 8.4 GHz (top right), and 15.3 GHz (bottom) with polarization vectors superimposed. The contours are in percentage of the peak surface brightness and increase in steps of 2. The lowest contour and peak brightness for 5, 8, and 15 GHz are $\pm 0.085\%$ of 144 mJy beam^{-1}, $\pm 0.085\%$ of 140 mJy beam^{-1}, and $\pm 0.17\%$ of 106 mJy beam^{-1}, respectively. χ vectors for 5 and 8 GHz: 1 mas = 0.25 and 0.3 mJy beam^{-1}, respectively.

(Figure 5) which indicates that the Faraday rotating medium is not mixed with the main synchrotron-emitting jet. Furthermore, the low depolarization suggested by the DP estimates and the

strong dependence of polarization angles on the square of the observing wavelength, support the picture of a Faraday screen with a relatively constant Faraday depth. Since the
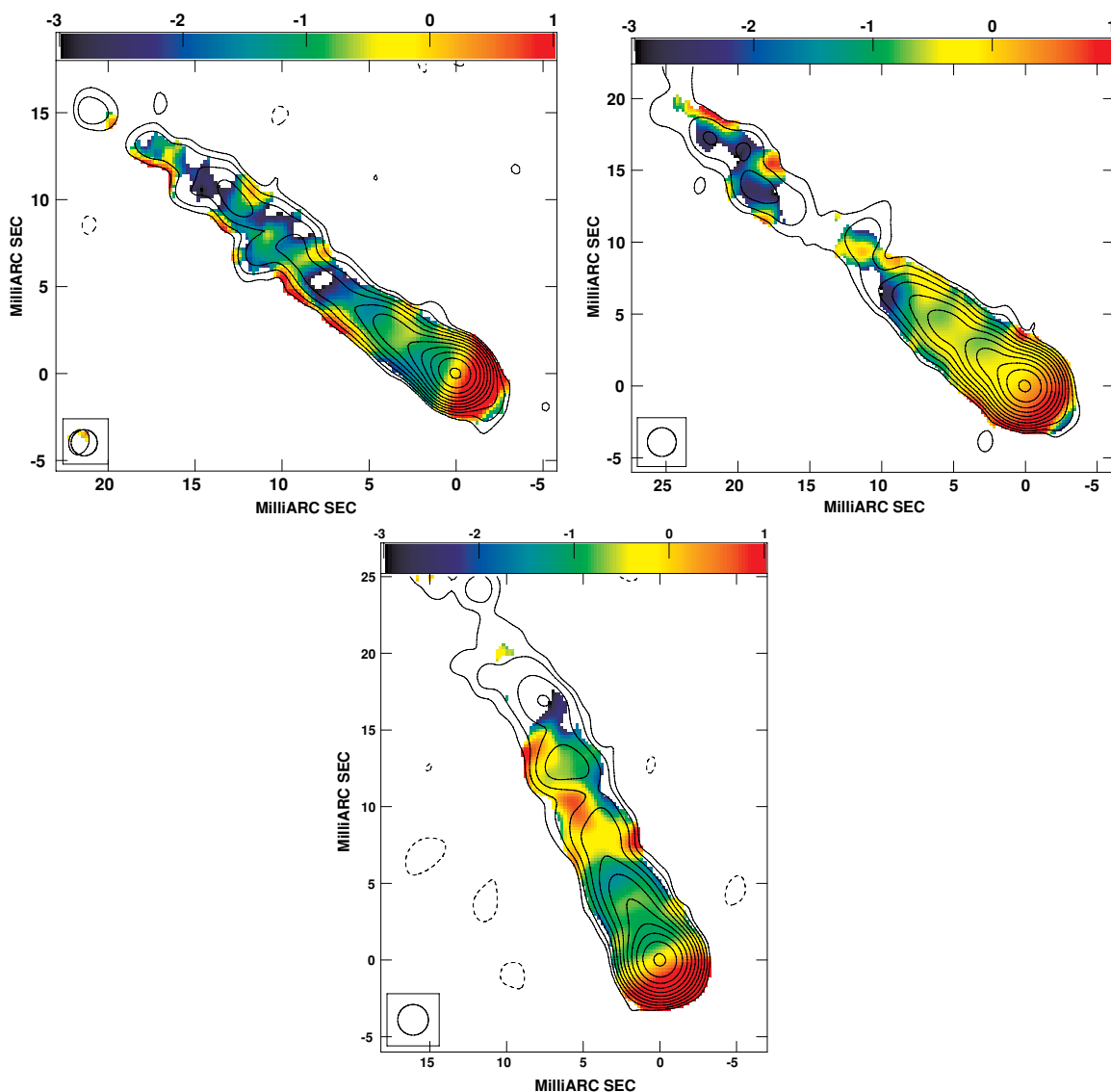
Figure 4. 5–8 GHz spectral-index map of (top left) 3C66B made with a 1.5 mas circular beam, (top right) 3C78 and (bottom) 3C264, each made with a 2 mas circular beam. The 5 GHz total intensity contours are superimposed. Note the optically thin counterjet emission in 3C66B and 3C78.

(A color version of this figure is available in the online journal.)

hot gas observed in X-rays in fact requires a highly tangled magnetic field to produce the observed RM, which does not seem to be borne out by the depolarization measurements, we suggest that an optically thin layer surrounding the jet that has sufficient thermal electrons mixed in with any synchrotron-emitting electrons could be a good candidate for the Faraday screen.

Sheaths around jets have been suggested to be present in both FRI and FRII jets on both kiloparsec (Hardcastle et al. 1996; Katz-Stone et al. 1999) and parsec-scales (Attridge et al. 1999; Kharb et al. 2008). Either shearing due to the jet interaction with the ambient medium or the presence of an intrinsic toroidal or helical magnetic field could result in these sheaths having ordered magnetic fields (Laing 1981; Lyutikov et al. 2005). Although a sheath resulting from jet entrainment has often been proposed for FRI jets (De Young 1984; Bicknell 1996); sheaths could also result from the diffusion of particles out of the beam into the external medium (O'Dea & Owen 1987) or from material associated with the inner part of a disk wind (Blandford & Levinson 1995; Hanasz & Sol 1996). The fact

that we observe similar parsec-scale jet RMs in FRIs and FRIIs, where the levels of entrainment are expected to differ (e.g., De Young 1993), appears to provide a support to the latter two models, under the assumption that jetlike magnetic field lines also thread the sheath region.

The most natural interpretation for the RM gradient observed in 3C78 is that it is due to a helical or toroidal jet magnetic field (Blandford 1993; Laing 1996). This is also consistent with the increase in the degree of polarization toward the edge of the jet (Figure 6). The asymmetry in the RM values is likely to be the combined effect of the jet orientation and the pitch angle of the field (for example, see Asada et al. 2002). Similar RM gradients have been observed in a number of other AGNs, including several BL Lac objects (Asada et al. 2002; Gabuzda et al. 2004, 2008; Zavala & Taylor 2005). Thus, the RM gradient together with the large rotation in the polarization angles and the low depolarization supports the idea that the Faraday rotating medium is a "sheath" around the parsec-scale jet, which is threaded by a helical magnetic field that is intrinsically associated with the jet.
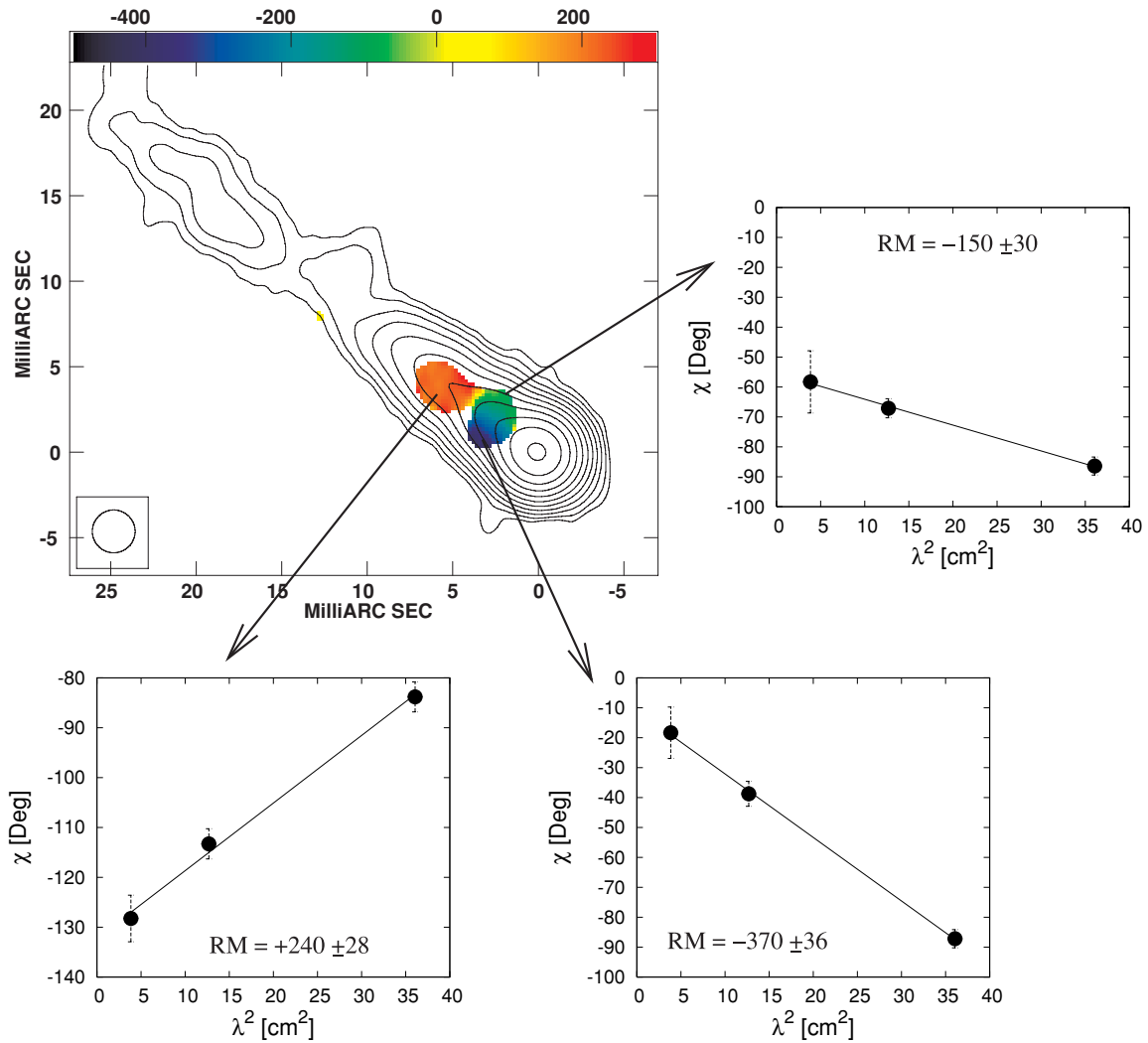
Figure 5. Three-frequency RM image of 3C78 with 5 GHz total intensity contours superimposed. An area covering four pixels (pixel size=0.2 mas) was used to create the inset χ-λ^2 plots. The RM values in the inset plots and color scale are in units of rad m^{-2}, with $\sigma_{RM} < 55$ rad m^{-2}. RMs in the rest frame of the source are larger by a factor $(1+z)^2$ or 1.058.

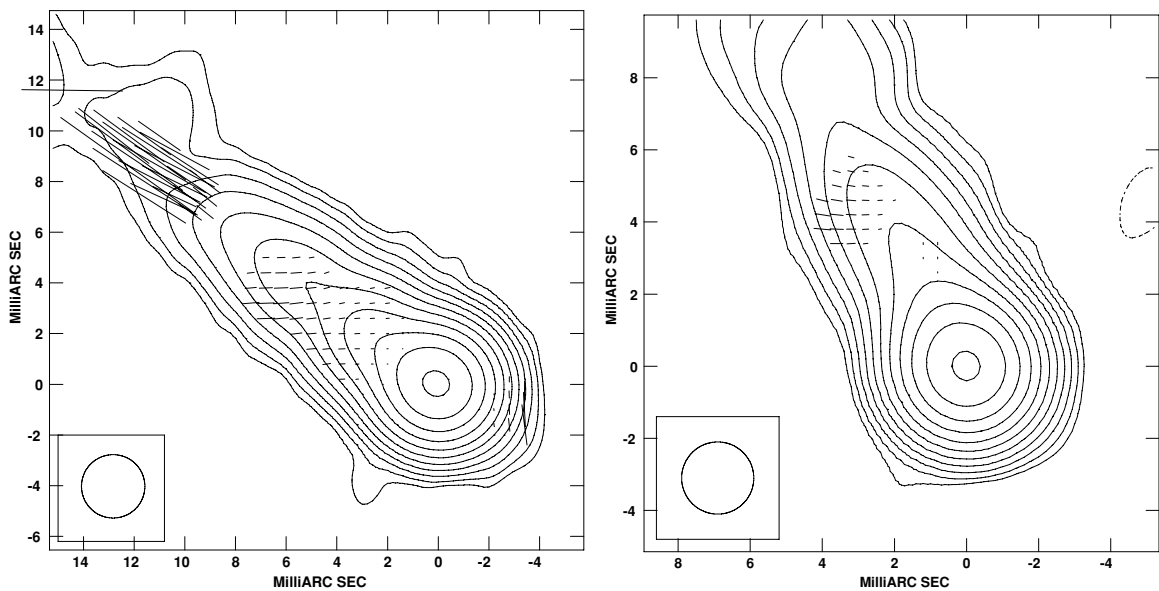(A color version of this figure is available in the online journal.)

Figure 6. 5 GHz total intensity contours with degree of polarization vectors superimposed for 3C78 (left) and 3C264 (right). 1 mas ticks correspond to 8% and 50% for 3C78 and 3C264, respectively. Degree of polarization clearly increases toward the southern and eastern edge of the 3C78 and 3C264 jets, respectively.
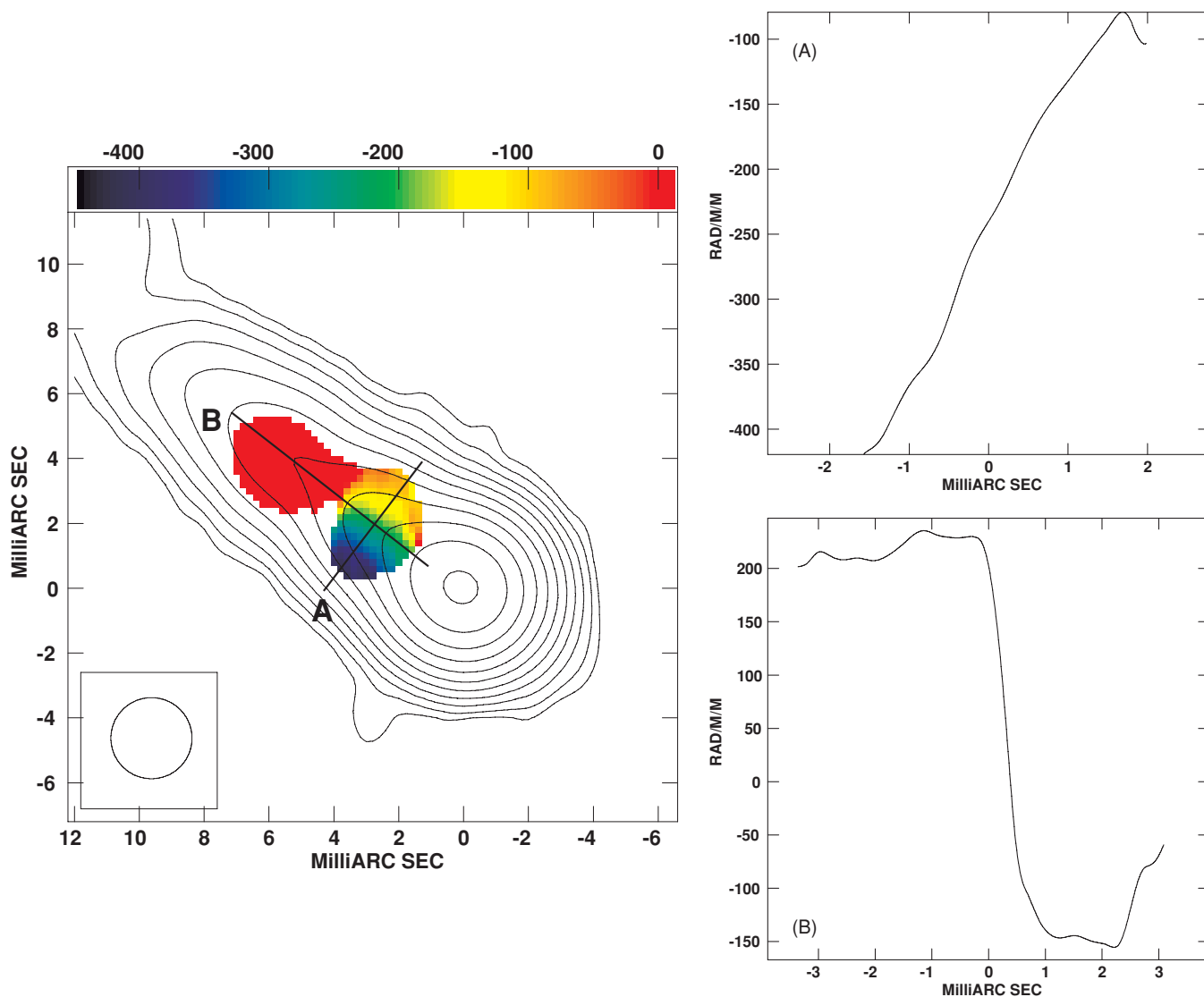
Figure 7. RM gradient across the jet in 3C78. The left panel zooms in and displays a narrower range of RM where the RM gradient is clearly visible perpendicular to the jet close to the core. The RM changes from ~-450 to ~-50 rad m^{-2} over a region 5 mas (two beam sizes) across the jet (Inset A). Inset B displays the RM along the jet direction. RMs in the rest frame of the source are larger by a factor $(1+z)^2$ or 1.058.

(A color version of this figure is available in the online journal.)

The electron density in the medium producing the Faraday rotation can be derived under the assumption that the condition of "equipartition" between the magnetic field and electron energy density (Burbidge 1959) holds in the radio jet (e.g., Feigelson et al. 1995; Harris & Krawczynski 2002). Using the 5 GHz jet flux density and volume we obtained the magnetic field strength, electron energy density, and pressure (Table 3) under the "equipartition" condition (see O'Dea & Owen 1987). For these calculations, we assumed the ratio of the relativistic proton to relativistic electron energy to be unity. The radio spectrum was assumed to extend from 10 MHz to 100 GHz. An average spectral index of 0.8 and a volume filling factor of unity were adopted for the jet. The constant C_{12} (Pacholczyk 1970) which depends on the spectral index and frequency cutoffs was taken to be 6.5×10^7.

Assuming that the Faraday rotating medium was external to the synchrotron-emitting jet volume but close to it, with the magnetic field strength being similar to the jet "equipartition" B-field of $\sim$5 mG a canonical rest-frame RM of 200 rad m^{-2}

and a path length of 1 pc, we derive a lower limit to the electron density which is a few times 0.01 cm^{-3} for the medium in 3C78 and 3C264. If we assume that the path length is in fact the width of an outer sheath layer, which is (say) about 10% of the jet width ($\approx$5 pc, estimated from the 5 GHz maps), we obtain an electron density of $\sim$0.1 cm^{-3}, which is of the same order as the electron density of the hot gas in the galaxy centers. Therefore, if the sheath was a "mixing" layer between the jet and the surrounding hot gas, it could certainly have the required electron density, magnetic field strength, and path length, to produce the observed RM.

Although helical jet B-fields provide an attractive explanation for the transverse RM gradient and increase in fractional polarization at the jet edges in 3C78, alternative explanations, such as an inhomogeneous surrounding medium (e.g., accretion disk wind) that gives rise to a local enhancement in the RM on one side of the jet, cannot be completely ruled out. The absence of a clear transverse RM gradient in 3C78 further from the core may provide evidence for an inhomogeneous ambient medium,
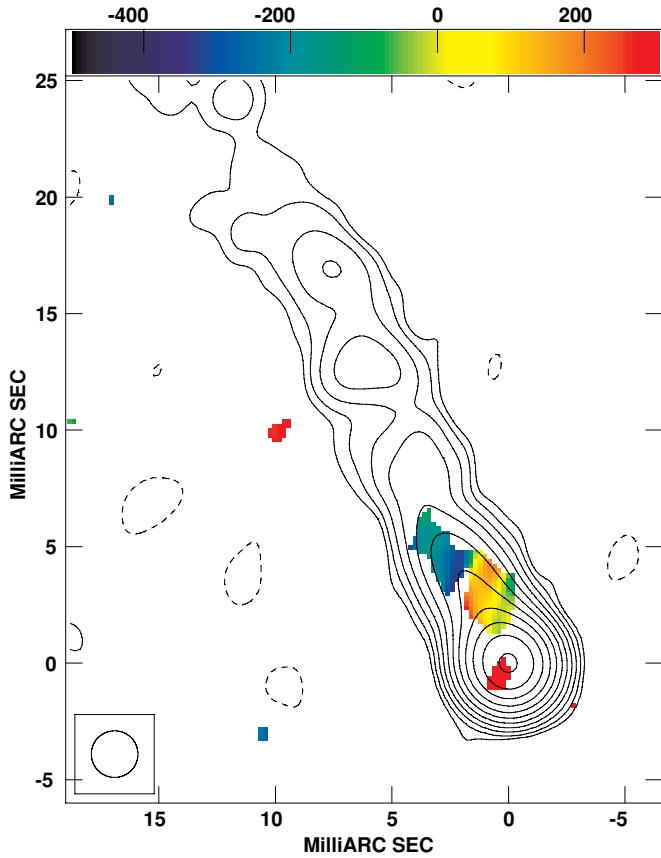
Figure 8. RM image of 3C264 with 5 GHz total intensity contours superimposed. Only the 5 and 8 GHz images were used to derive the RM. The color scale is in units of rad m^{-2} with σ_{RM} being typically < 50 rad m^{-2}. RMs in the rest frame of the source are larger by a factor $(1 + z)^2$ or 1.044.
(A color version of this figure is available in the online journal.)

whether or not this jet carries a helical B-field. The jet of 3C264 does not show any clear gradients in our two-frequency RM map, suggesting that either this jet does not carry a helical B-field or that if the jet does carry a helical field, this field is distorted by interaction with the surrounding medium. Higher-resolution low-frequency observations that are sensitive to Faraday rotation but better resolve the jet in the transverse direction, such as may be provided by future space VLBI projects, may help resolve these questions.

5.2.1. Clues from Optical Observations

The three FRIs under study have been observed with optical imaging polarimetry with the *HST* at a resolution of $\sim 0.1''$ (translating to scales of hundreds of parsecs for these sources) by Perlman et al. (2006) and Capetti et al. (2007). Perlman et al. (2006) found that 3C66B, 3C78, and 3C264 showed the simplest magnetic field structures among the six nearby radio galaxies studied. Interestingly, both 3C78 and 3C264 (sources with significant parsec-scale polarization) exhibit an increase in the degree of polarization along the edges of the optical jet. Perlman et al. (2006) suggested that such a magnetic field structure could arise due to a spine–sheath jet structure, with the sheath forming due to the interaction of the jet with the surrounding medium, which stretches the magnetic field lines due to shear. We note that a spine–sheath structure could also simply result from a helical jet magnetic field, with or without shearing (Lyutikov et al. 2005).

A "potential" problem with the jet interaction picture could be that on going down from $\sim 0.1''$ to mas scales, we detect polarization along the center of the jet (in 3C78 and 3C264) but not at the edges as expected from a "sheath". This could either be due to insignificant interaction/entrainment on parsec-scales, or, the existence of a helical magnetic field extending from parsecs (where its presence is revealed by the observed transverse RM gradient) to hundreds of parsecs (where its presence is revealed by the observed transverse optical polarization structure). This helical field could originate due to the rotation of the accretion disk plus jet outflow and propagate outward with the jet throughout its length. Another possibility is the scenario proposed by Asada et al. (2008b) for the quasar NRAO140, viz., that the jet has a spine–sheath structure with helical magnetic fields threading both the jet components, but the field is tightly wound in the sheath (resulting in the RM gradient) and loosely wound in the spine (leading to aligned magnetic fields in the inner jet). This scenario is also consistent with the findings in 3C120 and 3C166. Interestingly, such a magnetic field geometry has been known to result in the matter + Poynting flux dominated jets produced in the three-dimensional general relativistic MHD simulations of De Villiers et al. (2005) and Hawley & Krolik (2006). Such a magnetic field geometry could result in net depolarization at the jet edges which have transverse fields as opposed to the dominant spine which have aligned fields, thereby resolving the "potential" problem. Significant interaction/entrainment on scales of a few hundred parsecs, along with magnetic flux conservation could reproduce the

Table 1
Observed Parameters

Source	z	Scale (pc mas^{-1})	Freq (GHz)	I_{peak} (mJy bm^{-1})	I_{tot} (mJy)	I_{rms} (μJy bm^{-1})	P_{peak} (μJy bm^{-1})	P_{rms} (μJy bm^{-1})
3C66B	0.0212	0.424	5.0	113.9	186.2	43.4	$\cdots$	34.3
			8.4	110.1	193.2	46.9	636	37.5
			15.3	97.4	160.9	87.8	$\cdots$	66.6
3C78	0.0286	0.567	5.0	342.1	547.8	70.4	846	40.4
			8.4	330.9	548.1	64.7	993	39.8
			15.3	242.7	416.5	183.7	720	97.1
3C264	0.0217	0.433	5.0	144.4	191.6	47.5	578	39.8
			8.4	139.7	186.8	51.8	364	39.4
			15.3	106.3	142.1	96.3	$\cdots$	70.2

Notes. Column 1: source name. Column 2: redshift. Column 3: parsecs corresponding to 1 mas in the source. Column 4: observing frequency in GHz. Column 5: peak surface brightness in the total intensity (I) map. Column 6: Total VLBI flux density. Column 7: rms noise in the I map. Column 8: Peak surface brightness in the polarized intensity (P) map. Column 9: rms noise in the P map.
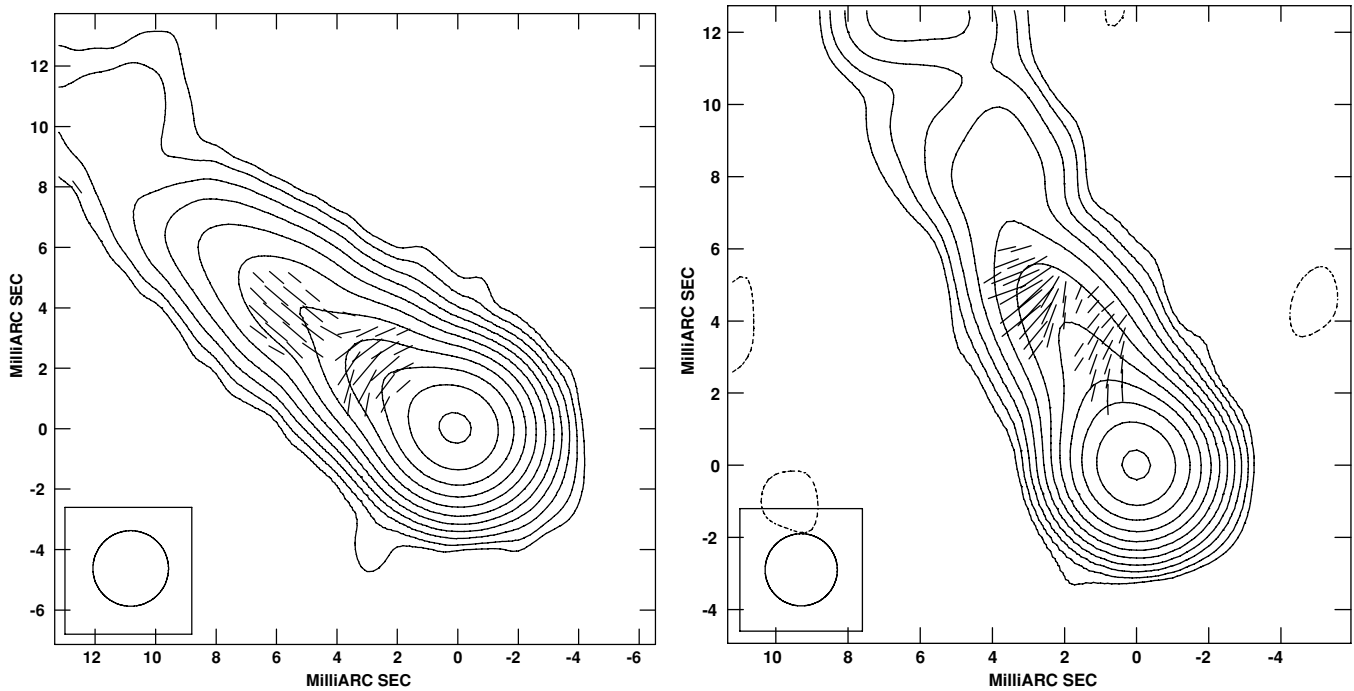
Figure 9. Polarization maps with 5 GHz total intensity contours of 3C78 (left) and 3C264 (right) with the effects of RM removed. Circular beams of 2.5 and 2.0 mas were used for the 3C78 and 3C264 maps, respectively. χ vectors for 3C78 and 3C264: 1 mas = 0.6 and 0.4 mJy beam^{-1}, respectively. The intrinsic EVPA for the jet in 3C78 changes from nearly longitudinal to nearly transverse to the VLBI jet direction, while it remains roughly transverse throughout in 3C264.

Table 2
Radio Galaxies with Measured Parsec-scale RMs

Source Name	FR Type	z	Int. RM rad m^{-2}	RM rad m^{-2}	Comment	Ref
3C78	I	0.0286	+14	−400, +200	In jet at r= 1.7, 4.3 pc	1
3C264[a]	I	0.0217	+16	−250, +150	In jet at r= 2.3, 1.9 pc	1
3C84	I	0.0175	... [b]	+7000	In jet at r= 5 pc	2
M87	I	0.0043	+872	−4500	In jet at r= 2 pc	3
3C111	II	0.0485	−19	−750, −200	In jet at r= 2.8, 4.7 pc	3
3C120	II	0.0330	−3	+100[c]	In jet at r= 1 pc	3
				+1500[d], +5000	In jet at r= 1, 2 pc	4
3C166	II	0.2449	+101[e]	−2300[f], −310[f]	In jet at r < 3.8, 7.6 pc	5

Notes. Comparison of FRI and FRII radio galaxies with parsec-scale RM measurements available at present. [a] Parsec-scale RM was obtained using only two frequencies, and is subject to the $\pm n\pi$ ambiguity. Column 4 lists the integrated RM from Simard-Normandin et al. (1981b). Column 5 lists the average RM at a projected distance r from the core.
[b] Unpolarized in Simard-Normandin et al. (1981a).
[c] Core RM of +2080 rad m^{-2} was detected in 3C120.
[d] Gomez et al. (2008) have suggested a time variability in the jet RM of 3C120.
[e] Integrated RM was estimated from values listed in Simard-Normandin et al. (1981a).
[f] Rest-frame RM, obtained by multiplying RM by $(1 + z)^2$=1.55 for 3C166.
References. (1) Present paper; (2) Taylor et al. (2006); (3) Zavala & Taylor (2002); (4) Gomez et al. (2008); (5) Taylor et al. (2001).

transverse B-field spine and longitudinal B-field sheath observed in kiloparsec-scale radio galaxy jets (Canvin et al. 2005; Laing et al. 2006).

Another interesting feature that emerges from optical observations is the presence of optical jets in the majority of radio galaxies with detected parsec-scale RMs, i.e., detected parsec-scale polarization over two or more radio frequencies, which in turn could be the result of low depolarization between frequencies. With the exception of 3C111 and 3C166, all the radio galaxies listed in Table 2 have optical jets. However, even 3C166 exhibits an optical "tail" along the radio jet direction (de Koff et al. 1996). Both 3C111 and 3C166 also exhibit unresolved *HST* nuclei which have been suggested to be the unresolved

bases of optical jets (Chiaberge et al. 2000). A possible connection between the presence of optical emission in the jet and detectable parsec-scale polarization in the radio needs to be examined further with a greater number of sources.

However if there was such a connection, it can easily be understood. Optical jet emission is expected to result from particle re-acceleration and to some extent, Doppler boosting (e.g., Sparks et al. 1994; Bicknell 1996). Two of the three FRIIs with detected polarized emission, viz., 3C111 and 3C120, are broad-line radio galaxies, and are likely to exhibit Doppler boosting in their jets due to being oriented at relatively small angles to line of sight. Furthermore, the kiloparsec-scale radio core prominence values of the three FRIs under study indicate

Table 3
Derived Parameters

Source	L_{rad} (erg s^{-1})	E_{min} (erg)	B_{min} (mG)	P_{min} (dynes cm^{-2})	n_e (cm^{-3})
3C66B	3.9E+40	6.9E+51	8.1	6.1E-06	⋯
3C78	2.1E+41	4.6E+52	7.1	4.7E-06	0.03
3C264	4.3E+40	1.2E+52	5.7	3.0E-06	0.04

Notes. Column 1: source name. Column 2: the averaged total radio luminosity. Columns 3 & 4: particle (electrons and protons) energy and magnetic field strength at the minimum pressure P_{min}, obtained assuming the "equipartition" condition. Column 5: minimum pressure. Column 6: electron density derived for an RM of 200 rad m^{-2} using the "equipartition" B-field strength and path length $dl = 1$ pc.

that the most polarized source, 3C78, is also the most core dominant, while the least polarized source, 3C66B, is the least core-dominant. This underscores the importance of Doppler boosting in these parsec-scale jets. Particle re-acceleration could occur in the jet shear layer or sheath, as the jet interacts with the surrounding medium, thereby producing a net deceleration and converting bulk kinetic energy into high-energy optical radiation (Owen et al. 1989; Stawarz & Ostrowski 2003).

6. SUMMARY AND CONCLUSIONS

We have observed three FRI radio galaxies, viz., 3C66B, 3C78, and 3C264, with polarization sensitive VLBI at 5, 8, and 15 GHz. We detected polarization in all three and obtained RMs across the parsec-scale jets of 3C78 and 3C264. RM was obtained using all the three frequencies in 3C78 but only two frequencies in 3C264, which is therefore subject to uncertainty due to $\pm n\pi$ ambiguities that cannot be resolved. To summarize,

1. Polarization was detected in the jets of 3C66B at 8 GHz, in 3C78 at all the three frequencies, and in 3C264 at 5 and 8 GHz.

2. The total intensity maps confirm the detection of a counterjet in 3C66B and indicate the presence of one in 3C78. The 5–8 GHz spectral-index maps reveal an optically thick core and an optically thin jet in all sources. The counterjet emission in 3C66B and 3C78 is also optically thin.

3. The parsec-scale jet RM in 3C78 ranges from ∼+200 rad m^{-2} to ∼ −400 rad m^{-2}. The core appears to be completely depolarized. An RM gradient is observed across the jet in 3C78 in a region that is over two beam sizes across. Furthermore, the degree of polarization increases along the edge of the jet. This strongly supports the idea of a helical jet magnetic field.

4. The polarization angles rotate by almost 90° between the three frequencies in 3C78. The depolarization parameter is close to unity in the jet, suggesting low depolarization at longer wavelengths. This suggests that the Faraday rotation is occurring in a layer containing thermal plasma that is external to the main body of the jet.

5. After correcting for the Faraday rotation, the magnetic field in 3C78 seems to be aligned with the jet direction close to the core, but becomes orthogonal further down the jet.

6.. The two-frequency parsec-scale RM in the 3C264 jet varies from ∼+250 rad m^{-2} to ∼ −300 rad m^{-2}. The core is completely depolarized.

7. The parsec-scale RMs in 3C78 and 3C264 are similar to those observed in other nearby FRI and FRII radio galaxies. Parsec-scale RM of a few hundred rad m^{-2} have also been inferred in the jets of the Doppler-beamed BL Lacs and quasars. The similar parsec-scale RMs in these AGN classes suggest an intrinsic origin, perhaps in the jet medium itself.

Based on the transverse RM gradient, increase in the degree of polarization toward the edge of the jet, large rotation of the polarization angles due to the Faraday rotation, and the small depolarization in 3C78, we argue that a layer surrounding the jet and carrying a helical magnetic field forms the Faraday screen. This suggestion is supported by *HST* optical polarization images. The recent work by Gomez et al. (2008) on 3C120 is likewise fully consistent with our conclusions.

The presence of optical jets in the majority of radio galaxies with detected parsec-scale polarization and the spine–sheath polarization structure observed in the *HST* polarization images of some of these sources suggests a simple connection: a sheath layer around the jet, produced either by jet–medium interaction or a helical magnetic field, is producing both. Jet–ISM entrainment and interaction could cause (1) mixing of thermal gas with the outer sheath layer of the jet which produces the RM, and (2) particle acceleration which produces the optical jet. This connection needs to be further explored based on a larger number of sources.

REFERENCES

Asada, K., Inoue, M., Kameno, S., & Nagai, H. 2008a, ApJ, 675, 79
Asada, K., Inoue, M., Nakamura, M., Kameno, S., & Nagai, H. 2008b, ApJ, 682, 798
Asada, K., Inoue, M., Uchida, Y., Kameno, S., Fujisawa, K., Iguchi, S., & Mutoh, M. 2002, PASJ, 54, L39
Attridge, J. M., Roberts, D. H., & Wardle, J. F. C. 1999, ApJ, 518, L87
Baum, S. A., Heckman, T. M., Bridle, A., van Breugel, W. J. M., & Miley, G. K. 1988, ApJS, 68, 643
Baum, S. A., Zirbel, E. L., & O'Dea, C. P. 1995, ApJ, 451, 88
Baum, S. A., et al. 1997, ApJ, 483, 178
Baum, S. A., et al. 1998, ApJ, 492, 854
Begelman, M. C. 1982, in IAU Symp. 97, Extragalactic Radio Sources Viscous Dissipation in Jets, ed. D. S. Heeschen & C. M. Wade (Dordrecht: Kluwer), 223
Bicknell, G. V. 1995, ApJS, 101, 29
Bicknell, G. V. 1996, in ASP Conf. Ser. 100, Energy Transport in Radio Galaxies and Quasars Decelerating Relativistic Jets and the Fanaroff–Riley Classification, ed. P. E. Hardee, A. H. Bridle, & J. A. Zensus (San Francisco, CA: ASP), 253
Blandford, R. D. 1993, in . Space Telescope Science Inst. Symp. Ser. 6, Astrophysical Jets, (Cambridge: Cambridge Univ. Press), 15
Blandford, R. D., & Levinson, A. 1995, ApJ, 441, 79
Burbidge, G. R. 1959, ApJ, 129, 849
Burn, B. J. 1966, MNRAS, 133, 67
Canvin, J. R., Laing, R. A., Bridle, A. H., & Cotton, W. D. 2005, MNRAS, 363, 1223
Capetti, A., Axon, D. J., Chiaberge, M., Sparks, W. B., Duccio Macchetto, F., Cracraft, M., & Celotti, A. 2007, A&A, 471, 137

Chiaberge, M., Capetti, A., & Celotti, A. 1999, A&A, 349, 77
Chiaberge, M., Capetti, A., & Celotti, A. 2000, A&A, 355, 873
Cioffi, D. F., & Jones, T. W. 1980, AJ, 85, 368
Crane, P. E. A. 1993, ApJ, 402, L37
Croke, S. M., & Gabuzda, D. C. 2008, MNRAS, 386, 619
Croston, J. H., Hardcastle, M. J., Birkinshaw, M., & Worrall, D. M. 2003, MN-RAS, 346, 1041
de Koff, S., Baum, S. A., Sparks, W. B., Biretta, J., Golombek, D., Macchetto, F., McCarthy, P., & Miley, G. K. 1996, ApJS, 107, 621
de Koff, S., et al. 2000, ApJS, 129, 33
De Villiers, J.-P., Hawley, J. F., Krolik, J. H., & Hirose, S. 2005, ApJ, 620, 878
De Young, D. S. 1984, in Physics of Energy Transport in Extragalactic Radio Sources, Proc. NRAO Workshop no. 9, Greenk Bank, WV, July 30–August 3, ed. A. H. Bridle (Green Bank, WV: NRAO), 202
De Young, D. S. 1993, ApJ, 405, L13
De Young, D. S. 1996, in ASP Conf. Ser. 100, Energy Transport in Radio Galaxies and Quasars Boundary Layer Development, Entrainment, and Energy Transport in Radio Sources, ed. P. E. Hardee, A. H. Bridle, & J. A. Zensus (San Francisco, CA: ASP), 261
Fanaroff, B. L., & Riley, J. M. 1974, MNRAS, 167, 31P
Feigelson, E. D., Laurent-Muehleisen, S. A., Kollgaard, R. I., & Fomalont, E. B. 1995, ApJ, 449, L149
Fraix-Burnet, D. 1997, MNRAS, 284, 911
Gabuzda, D. C., Murray, É., & Cronin, P. 2004, MNRAS, 351, L89
Gabuzda, D. C., Pushkarev, A. B., & Garnich, N. N. 2001, MNRAS, 327, 1
Gabuzda, D. C., Vitrishchak, V. M., Mahmud, M., & O'Sullivan, S. P. 2008, MNRAS, 384, 1003
Gardner, F. F., & Whiteoak, J. B. 1966, ARA&A, 4, 245
Giovannini, G., Cotton, W. D., Feretti, L., Lara, L., & Venturi, T. 2001, ApJ, 552, 508
Gomez, J., Marscher, A. P., Jorstad, S. G., Agudo, I., & Roca-Sogorb, M. 2008, ApJ, 681, L69
Hanasz, M., & Sol, H. 1996, A&A, 315, 355
Hardcastle, M. J., Alexander, P., Pooley, G. G., & Riley, J. M. 1996, MNRAS, 278, 273
Hardcastle, M. J., Birkinshaw, M., & Worrall, D. M. 2001, MNRAS, 326, 1499
Harris, D. E., & Krawczynski, H. 2002, ApJ, 565, 244
Hawley, J. F., & Krolik, J. H. 2006, ApJ, 641, 103
Junor, W., Biretta, J. A., & Wardle, J. F. C. 2001, in IAU Symp., VLBA Lambda Lambda 6, 4 cm Polarimetry of Vir A, ed. R. T. Schilizzi (Dordrecht: Kluwer), 136
Katz-Stone, D. M., Rudnick, L., Butenhoff, C., & O'Donoghue, A. A. 1999, ApJ, 516, 716
Kharb, P., Gabuzda, D., & Shastri, P. 2008, MNRAS, 384, 230
Kharb, P., & Shastri, P. 2004, A&A, 425, 825
Kharb, P., Shastri, P., & Gabuzda, D. C. 2005, ApJ, 632, L69
Killeen, N. E. B., Bicknell, G. V., & Ekers, R. D. 1986, ApJ, 302, 306
Laing, R. A. 1981, ApJ, 248, 87
Laing, R. A. 1996, in ASP Conf. Ser. 100, Energy Transport in Radio Galaxies and Quasars Brightness and Polarization Structure of Decelerating Relativistic Jets, ed. P. E. Hardee, A. H. Bridle, & J. A. Zensus (San Francisco, CA: ASP), 241

Laing, R. A., Canvin, J. R., Bridle, A. H., & Hardcastle, M. J. 2006, MNRAS, 372, 510
Lobanov, A. P. 1998, A&A, 330, 79
Lyutikov, M., Pariev, V. I., & Gabuzda, D. C. 2005, MNRAS, 360, 869
Mathews, W. G., & Brighenti, F. 2003, ARA&A, 41, 191
Matthews, T. A., Morgan, W. W., & Schmidt, M. 1964, ApJ, 140, 35
McCarthy, P. J., van Breugel, W., Spinrad, H., & Djorgovski, S. 1987, ApJ, 321, L29
Middelberg, E. 2004, PhD thesis, AA(Max-Planck Institut für Radioastronomie Auf dem Hügel, 69 53121 Bonn, Germany)
Nan, R., Gabuzda, D. C., Kameno, S., Schilizzi, R. T., & Inoue, M. 1999, A&A, 344, 402
Nan, R. D., Zhang, H. Y., Gabuzda, D. C., Ping, J. S., Schilizzi, R. T., Tian, W. W., & Inoue, M. 2000, A&A, 357, 891
Netzer, H., & Laor, A. 1993, ApJ, 404, L51
O'Dea, C. P., & Owen, F. N. 1985, AJ, 90, 954
O'Dea, C. P., & Owen, F. N. 1987, ApJ, 316, 95
Owen, F. N., Hardee, P. E., & Cornwell, T. J. 1989, ApJ, 340, 698
Owen, F. N., & Laing, R. A. 1989, MNRAS, 238, 357
Pacholczyk, A. G. 1970, in Radio Astrophysics. Nonthermal Processes in Galactic and Extragalactic Sources. Series of Books in Astronomy and Astrophysics, (San Francisco, CA: Freeman)
Perlman, E. S., et al. 2006, ApJ, 651, 735
Privon, G. C., O'Dea, C. P., Baum, S. A., Axon, D. J., Kharb, P., Buchanan, C. L., Sparks, W., & Chiaberge, M. 2008, ApJS, 175, 423
Reynolds, C., Cawthorne, T. V., & Gabuzda, D. C. 2001, MNRAS, 327, 1071
Rowan-Robinson, M. 1995, MNRAS, 272, 737
Rudnick, L., & Jones, T. W. 1983, AJ, 88, 518
Schombert, J. M. 1986, ApJS, 60, 603
Simard-Normandin, M., Kronberg, P. P., & Button, S. 1981a, ApJS, 46, 239
Simard-Normandin, M., Kronberg, P. P., & Button, S. 1981b, ApJS, 45, 97
Sparks, W. B., Biretta, J. A., & Macchetto, F. 1994, ApJS, 90, 909
Sparks, W. B., Golombek, D., Baum, S. A., Biretta, J., de Koff, S., Macchetto, F., McCarthy, P., & Miley, G. K. 1995, ApJ, 450, L55
Stawarz, Ł., & Ostrowski, M. 2003, New Astron. Rev., 47, 521
Tadhunter, C. N., Morganti, R., di Serego-Alighieri, S., Fosbury, R. A. E., & Danziger, I. J. 1993, MNRAS, 263, 999
Tansley, D., Birkinshaw, M., Hardcastle, M. J., & Worrall, D. M. 2000, MNRAS, 317, 623
Taylor, G. B. 1998, ApJ, 506, 637
Taylor, G. B., Gugliucci, N. E., Fabian, A. C., Sanders, J. S., Gentile, G., & Allen, S. W. 2006, MNRAS, 368, 1500
Taylor, G. B., Hough, D. H., & Venturi, T. 2001, ApJ, 559, 703
Udomprasert, P. S., Taylor, G. B., Pearson, T. J., & Roberts, D. H. 1997, ApJ, 483, L9
Urry, C. M., & Padovani, P. 1995, PASP, 107, 803
Verdoes Kleijn, G. A., Baum, S. A., de Zeeuw, P. T., & O'Dea, C. P. 2002, AJ, 123, 1334
Walker, R. C., Benson, J. M., & Unwin, S. C. 1987, ApJ, 316, 546
Zavala, R. T., & Taylor, G. B. 2002, ApJ, 566, L9
Zavala, R. T., & Taylor, G. B. 2003, ApJ, 589, 126
Zavala, R. T., & Taylor, G. B. 2004, ApJ, 612, 749
Zavala, R. T., & Taylor, G. B. 2005, ApJ, 626, L73